Authors' Response to Reviews of

Large-scale forest stand height mapping in the northeastern U.S. and China using L-band spaceborne repeat-pass InSAR and GEDI LiDAR data

Yanghai Yu, Yang Lei, Paul Siqueira, Xiaotong Liu, Denuo Gu, Anmin Fu, Yong Pang, Wenli Huang, Jiancheng Shi

**RC: Reviewers' Comments**, AR: Authors' Response, ☐ Manuscript Text

## Reply to the first reviewer:

**RC: Estimating forest height from InSAR and spaceborne lidar data over large areas are challenging but meaning work. However, the presentation of this manuscript makes it even more challenging to understand than it should be. Here are some comments that may be helpful!**

AR: Thanks very much to the reviewer for the recognition and valuable comments! The specific response and revision are listed below.

**RC: 1. Line 50: repeat "sensitive to".**

AR: Thanks for noting this typo. We have corrected this in the revised version at line 52, as shown below.

> …LiDAR and SAR are promising for capturing the internal vertical structure of forests: LiDAR is fundamentally sensitive to structural details, while radar detects the three-dimensional distribution of vegetation elements (Ulaby et al., 1990).…

**RC: 2. Line 70: use footprint instead of point. Point can be confused by lidar point cloud.**

AR: Thanks for this good suggestion. We have fixed it in the revised version at line 70:

> …However, GEDI collects only discrete footprint measurements, spaced approximately 60 meters apart in the along-track direction and 600 meters apart in the cross-track direction…

**RC: 3. Figure 2 and related text: Why not using Landsat/Sentinel based disturbance detection results, directly?**

AR: This is an insightful suggestion. The goal of this paper is to develop a self-contained inversion framework for large-scale forest height estimation by fully leveraging the Radar-LiDAR fusion. In our approach, the SAR backscatter-based forest height inversion (for heights below 10 m) replaces the InSAR coherence-based estimates. Furthermore, the openly accessible annual ALOS-2 backscatter mosaic products facilitate forest height estimation for short vegetation or bare surfaces after forest disturbance. In this way, land cover changes from forests into short vegetation and bare surfaces will be included in the SAR backscatter-based forest height estimates. To demonstrate this approach, we tested how forest disturbances identified from Landsat/Sentinel-based disturbance products (used as ground truth benchmarks) emerges in the backscatter-based forest height pixels (<10 m). The experimental result showed that the SAR backscatter-based approach can effectively detect the majority of forest disturbances with comparable accuracy (>70%).

While optical-based products offer complementary insights, their direct integration could introduce additional artifacts or uncertainties, possibly in persistently cloud-covered regions. As the main scope of this paper is not to fully address the forest disturbance, we kindly ask for the reviewer's understanding that we do not introduce the optical-based products in current inversion framework.

**RC: Line 235 and equations: what does the a on the left mean? looks very similar to a. Suggest changing to other symbol. Also, where is hv(t2) ?**

AR: We feel sorry to create such confusion. This symbol is changed to the "$G$" to enhance the major distinction from symbol "a" at line 453 after revision. $h_v(t_2)$ represents the forest height after growth. However, the forest growth rate (although it can be derived by comparing the before/after status) can be modelled depending on the status of forest at either epoch, e.g., the initial forest height $h_v(t_1)$ in this work. Accordingly, this explanation is added at line 450 after revision as follows:

> …where $h_v$ represents the time-dependent forest height, $t_1, t_2$ denote the initial and later epochs, respectively. Although the forest growth rate is derived by comparing pre- and post-growth states, it can be modelled based only on forest height data from either epoch, for example, using the initial forest height $h_v(t_1)$:
>
> $$G = a \cdot h_v(t_1) + b \quad \textbf{(1)}$$
>
> Where $a$ and $b$ are linear coefficients. If a dense time-series of forest height data over certain forest land cover is provided, the above equation can be constructed in a differential form as:…

**RC: Line 245: It seems to be a typical tree height based allometric equation. But the parameters would vary a lot among tree species, and the forest age, determined by both t1, and t2. How were these uncertainties addressed?**

AR: We fully agree with this insight. Forest growth rates are inherently species-dependent. However, obtaining species-specific growth rates for individual trees across large regions remains impractical.

To address this limitation, from a modeling perspective, we developed a modified model incorporating forest growth dynamics, simulating its behavior using statistical growth functions derived from spaceborne ICESat-1 and GEDI datasets. Simulations reveal that the modified signal model can be effectively approximated by the original model at regional scales through local fitting, provided the adaptive parameters $S'$ and $C'$ are used to account for growth-induced variability (Figures 11 and 12 as shown below).

From a practical inversion perspective, we remark that the growth functions themselves were not directly employed in the inversion; instead, the original sinc model but with updated parameters ($S'$, $C'$) is used in the actual application to approximate the modified model taking natural growth into account.

To clarify this, we have added statements at line 471 as follows:

> …From a practical inversion perspective, the application of the modified model requires precise detailed statistics of natural growth across various forest types on a large scale. However, such data are currently unavailable, as existing spaceborne LiDAR datasets lack collocated measurements from two distinct time periods. In the absence of comprehensive forest growth data, this model is not yet recommended for direct large-scale use. Instead, it can be integrated into the framework of the original model by adjusting temporal parameters. The following subsection provides simulation examples to demonstrate this adaptation…

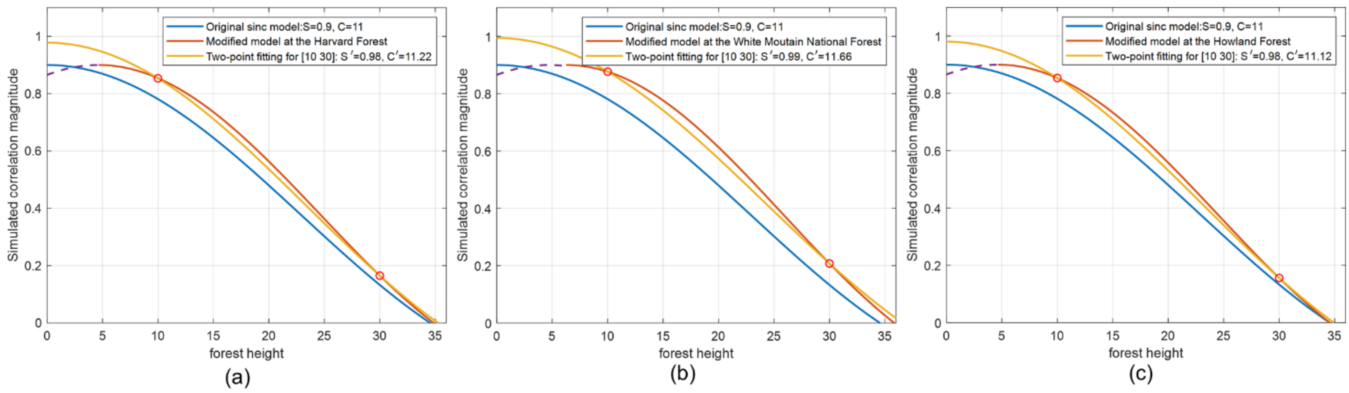


**Figure 11: Approximating the modified sinc model with the original model by aligning two points at 10 and 30 m: the newly fitted parameters at (a) Harvard Forest sites; (b) the forest site in Vermont; (c) Howland Forest site. The y-axis represents the coherence magnitude estimated from Equation (3) and (15).**

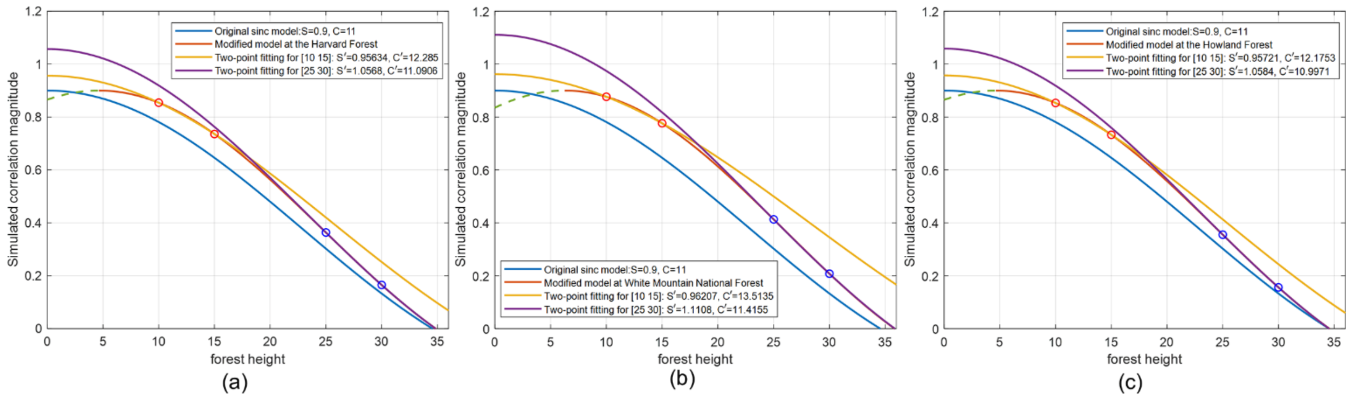


**Figure 12: Approximating the modified sinc model with the original model by aligning two points either at 10 and 15 m or at 25 and 30 m: the newly fitted parameters at (a) the Harvard Forest site; (b) the White Mountain National Forest site; (c) the Howland Forest site. The y-axis represents the coherence magnitude estimated from Equation (3) and (15).**

**RC: Line 250: What is the sinc model for? Whether I missed it, or it failed to be introduced clearly. But it seems to be a very important one. Not clear how the values in the y axis of Figure 4 were calculated?**

AR: Thank you for highlighting this oversight. The sinc function was omitted in the initial formulation and has now been added into the revised manuscript (Section 3.4.2, Line 459) as follows:

$$\left|\gamma_{t\&v}^{HV}(t_1)\right| = S(t_1) \cdot \mathrm{sinc}\left(\frac{h_v(t_2) - b \cdot dt}{(1 - a \cdot dt) \cdot C(t_1)}\right) \quad \textbf{(2)}$$

where $\left|\gamma_{t\&v}^{HV}(t_1)\right|$ represents the InSAR coherence at initial time $t_1$, it follows the model is shifted and scaled with respect to the original model (3), $dt = t_2 - t_1$.

The y-axis values are calculated using Equations (3) and (15). We understand that this information is not clearly explained in the original text. To address this, we have added their explanations in the relevant figure captions for Figures 10, 11, and 12, as follows:

**Figure 10, 11, and 12: … The y-axis represents the coherence magnitude estimated from Equation (3) and (15).**

**RC: Figure 3: Again, as shown in Fig 3b, the growth rate varied a lot among site (species, age, and site condition). Also in Fig 3a, it should be a combined results of many different growth rates. These results further demonstrate it is unreasonable to apply a global model for the entire regions, even just for the New England region.**

AR: We appreciate this valuable insight. As clarified above, a single global forest growth model cannot adequately capture the forest growth dynamics across diverse bioregions. To address this, we developed a modified model to represent the natural forest growth process and compared its behavior with that of the original model in Figure 11 and 12 now. In terms of practical inversion, through local fitting procedures (as verified by simulation), we demonstrate that the original model framework can approximate the modified model with updated parameters. Therefore, the original inversion framework is actually used in the large-scale application without introducing growth functions.

**RC: 2.2.3: Oops, I got lost after the sinc model. Sorry.**

AR: We apologize for the confusion in the descriptions of the original and updated models. For clarification, we have added the sentences to illustrate the main objective of this subsection at line 490 as follows:

…Without detailed forest growth statistics, this subsection demonstrates the modified sinc model can be well approximated in the framework of the original sinc model but with updated parameters $(S', C')$ using simulation. This enables the large-scale application achieved in the framework of original model without detailed forest growth statistics…

**RC: Figure 9: The flowchart definitely should come first, as the Figure 1 or 2. Also, make it a more general and easy to understand for general readers.**

AR: Thank you for your constructive suggestion. In response to your feedback, we have repositioned the revised methodological flowchart to the beginning of Section 3 (now Figure 5), and modify it using more generalized description:

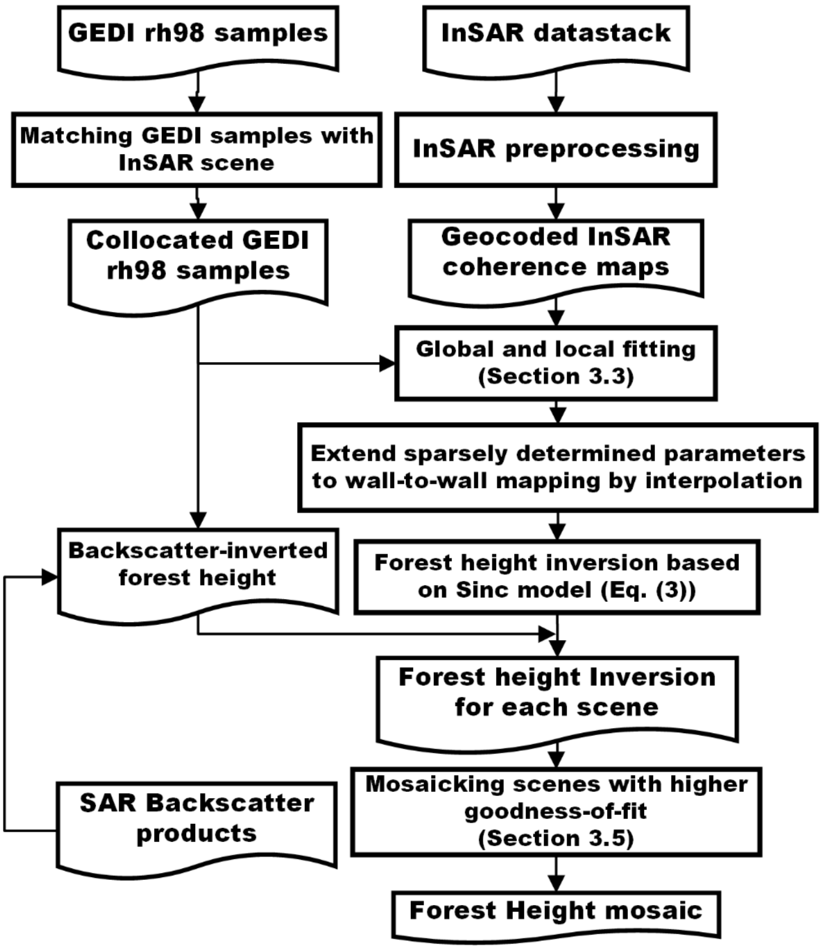


**Figure 5: Block diagram of the workflow for generating forest height mosaic.**

**RC: Figure 10: Labels on the color bar are too small to read. I would also suggest zoom into a few sub-figures of the study areas to show more details.**

AR: We thank the reviewer for this valuable suggestion. In response, we have updated the original figure to include a zoomed-in subsection with bolded labels and text to enhance clarity. This revised version is now presented as Figure 6 in the manuscript as follows:

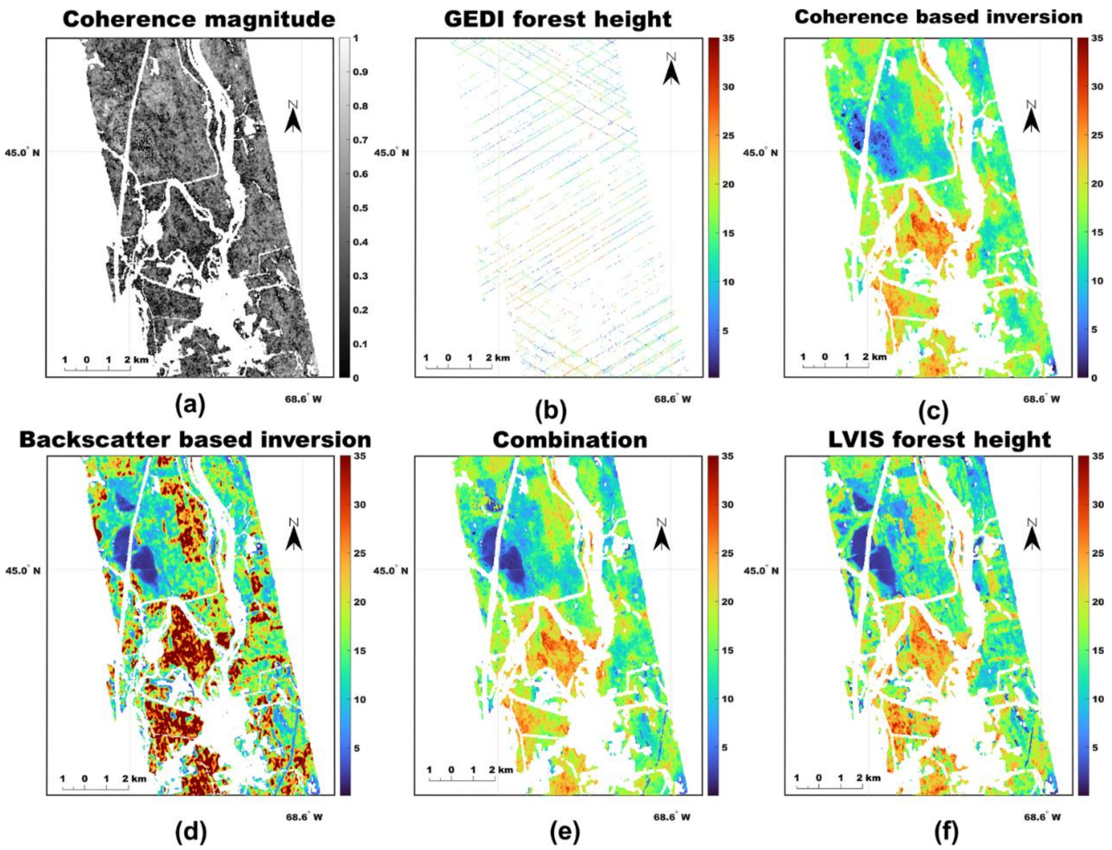


**Figure 6 An illustrative example of the processing steps at the Howland Forest site: (a) the input ALOS-1 coherence magnitude map; (b) the GEDI rh98 samples; (c) the forest height estimates based on InSAR coherence information; (d) the backscatter based height estimates; (e) the final forest height map after replacing the estimates of short trees in (c) with the collocated pixels in (d); (f) is the airborne LVIS LiDAR data for validation.**

**RC: Section 3: I would suggest put these parts before the methods.**

AR: Thanks for the good suggestion! Section 3 (now renumbered as Section 2) has been placed ahead of the methodology section.

**RC: Table 2 and 3: Please add hom many plot or how large is the validate site in the table2 and 3.**

AR: Thanks for the good suggestion. The relevant information has been updated in the Tables 1 and 2 in the revised manuscript as follows.

**Table 1 The forest validation sites covered by the airborne LiDAR observation in the New England, U.S**

| Validation sites | Location | Dominated tree species | LiDAR data acquisition year | Slope statistics | ALS validation area (ha) |
|---|---|---|---|---|---|
| Howland Forest | 68°44′ W, 45°12′N | Red spruce (Picea rubens Sarg.) and eastern hemlock | 2009 | Mean: 2.3° STD: 5.3 | $4.77\times 10^4$ |
| Harvard Forest | 72°11′W, 42°31′N | Red oak, Red maple, Black birch, White pine, Eastern hemlocc | 2021 | Mean: 5.5° STD: 4.6° | $4.87\times 10^4$ |
| White Mountain National Forest | 71°18′W, 44°6′N | Red Spruce, Eastern Hemlock, American Beech, and Red Maple, | 2011 | Mean: 9.7° STD: 8.6° | $1.20\times 10^4$ |
| Green Mountain National Forest | 73°04′W, 43°57′N | Sugar maple, American beech, red maple, yellow and paper birch | 2021 | Mean: 10.4° STD: 7.6° | $8.91\times 10^4$ |
| Naugatuck State Forest | 73°00′W 41°27′N | Northern red oak, Mixed upland hardwoods, Yellow-poplar | 2021 | Mean: 5.2° STD: 4.5° | $3.58\times 10^4$ |

**Table 2 The forest validation sites covered by the ALS validation data in northeastern China**

| Validation sites | Location | Dominated tree species | LiDAR data acquisition year | Slope statistics | ALS validation area (ha) |
|---|---|---|---|---|---|
| Mengjiagang Forest site | 130°42′E, 46°25′N | Coniferous plantations (Larix gmelinii and Pinus syvestris) | 2017 | Mean: 6.6° STD: 5.6° | $3.78\times 10^4$ |
| Dagujia Forest site | 125°00′E, 43°21′N | Coniferous plantations (Larix kaempferi, Pinus koraiensis, etc) | 2018 | Mean: 13.5° STD: 7.4° | $3.66\times 10^4$ |
| Saihanba Forest site | 117°18′E, 42°24′N | Larix principis-rupprechtii, Pinus syvestris, and Betula | 2018 | Mean: 8.7° STD: 7.3° | $2.98\times 10^4$ |
| Genhe Forest bureau | 121°32′E, 50°47′N | Larix gmelinii, Betula platyphylla, Populus davidiana | 2022 | Mean: 7.0° STD: 5.4° | $1.09\times 10^5$ |
| Hubao Forest site | 130°12′E, 43°28′N | Mongolian oak, Basswood, Betula platyphylla | 2018 | Mean: 8.7° STD: 7.4° | $3.99\times 10^5$ |

**RC: Fig 17,19,21,22,24,27,29, and so on. These figures are just too small to read clearly not to mention compare them. A good comparison should map the difference between the estimated and ground truth (ALS ERH98? maybe in Figure 29).**

AR: We sincerely apologize for the inconvenience during the visual interpretation of previous figures. To address this, we have carefully revised all relevant figures with bolded labels and text to enhance readability and interpretation as shown in Figures. 17, 18, 19, 20, 21, 22, 23, 24, 25, 26, 27, 28, 29, and 30 after revision (included at the end of this response). Additionally, we have updated differential height maps (include Figures 19, 23, 25, 28, and 30) between inversion and airborne validation data in the corresponding forest sites.

**RC: Conclusions: I would suggest have a longer discussion and a short conclusion in separate sections.**

AR: Thanks for this suggestion. All the limitations and implications for future works are discussed in the Section 5. The Sections 6 briefly concludes this paper.

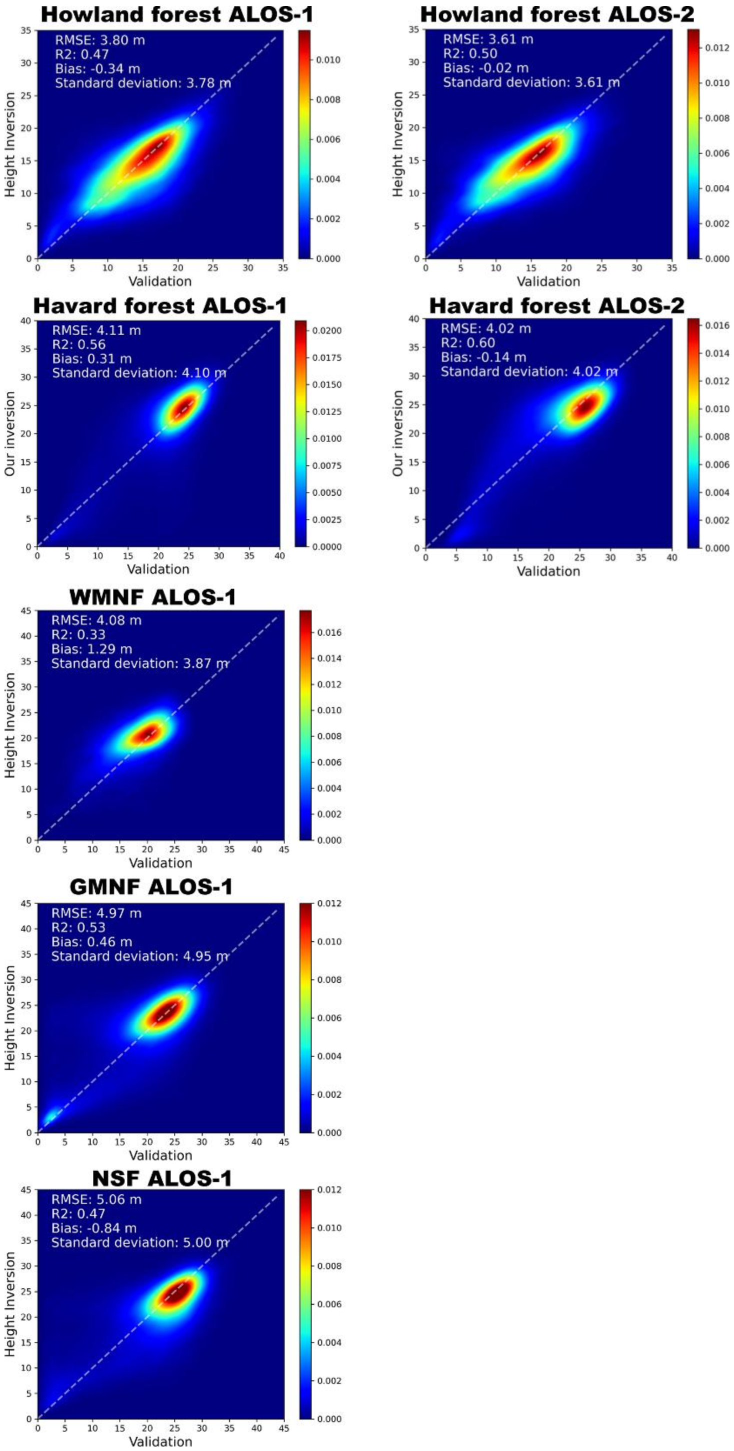


**Figure 17: Density scatterplots comparing LiDAR validation data with forest height inversion estimates across multiple sites of the New England: Left panels show ALOS-1-based estimates; right panels show ALOS-2-based estimates.**

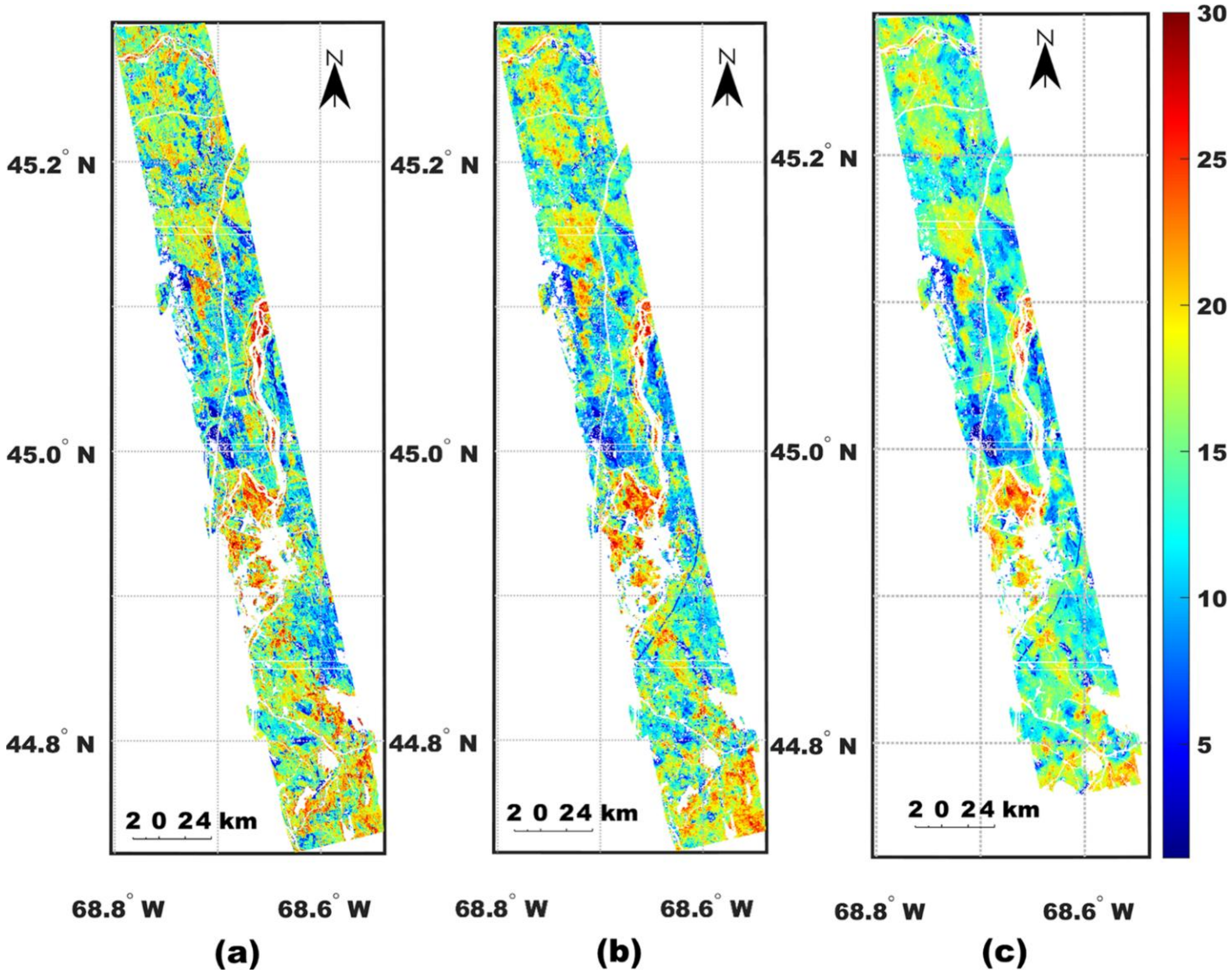


**Figure 18 Validation of forest height inversion results at the Howland Forest site: (a) LVIS RH98 canopy height map (30 m grid), (b) inversion extracted from ALOS-1 mosaic, and (c) ALOS-2 based inversion.**

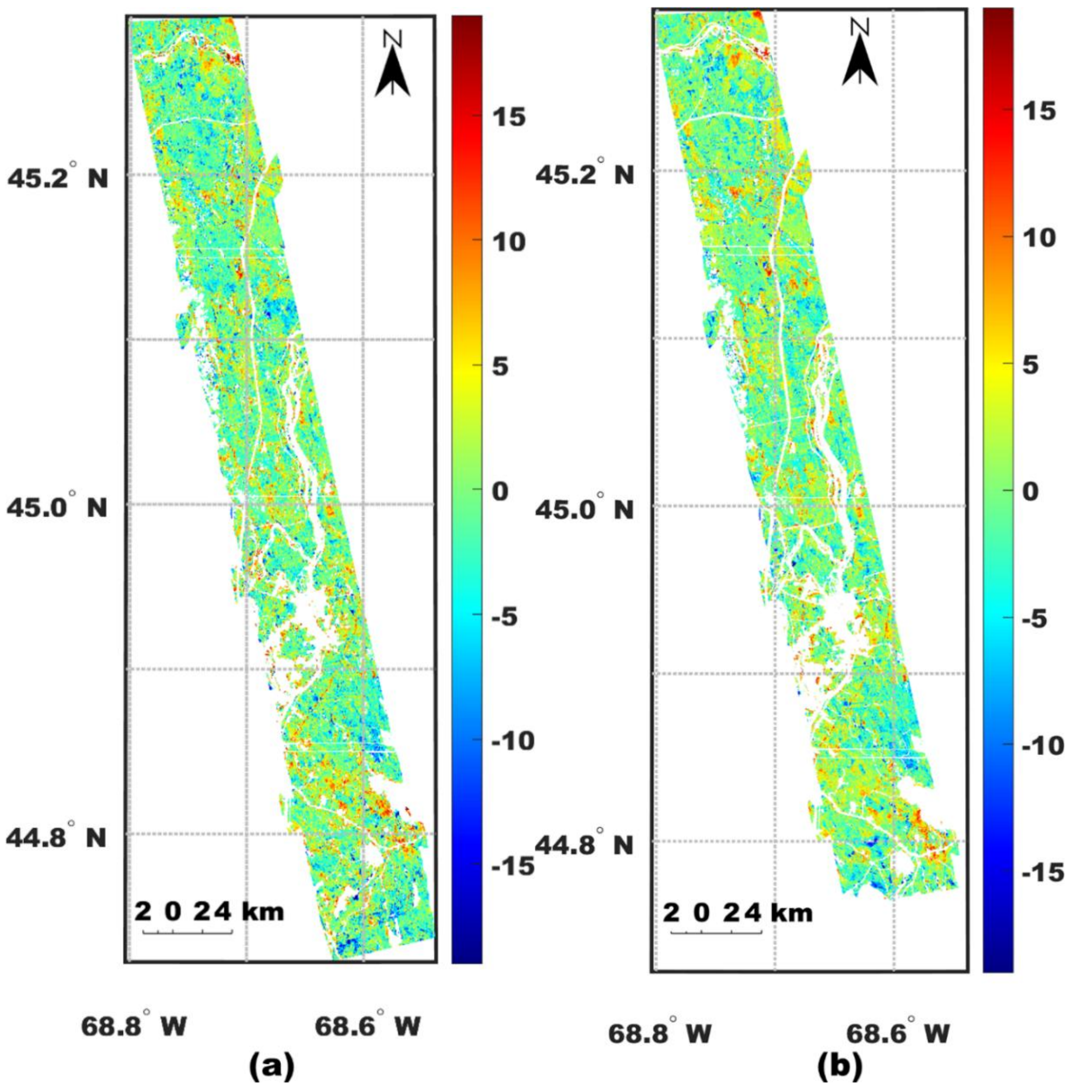


**Figure 19: The differential height maps of (a) ALOS-1 based inversion versus LVIS data and (b) ALOS-2 based inversion versus LVIS data.**

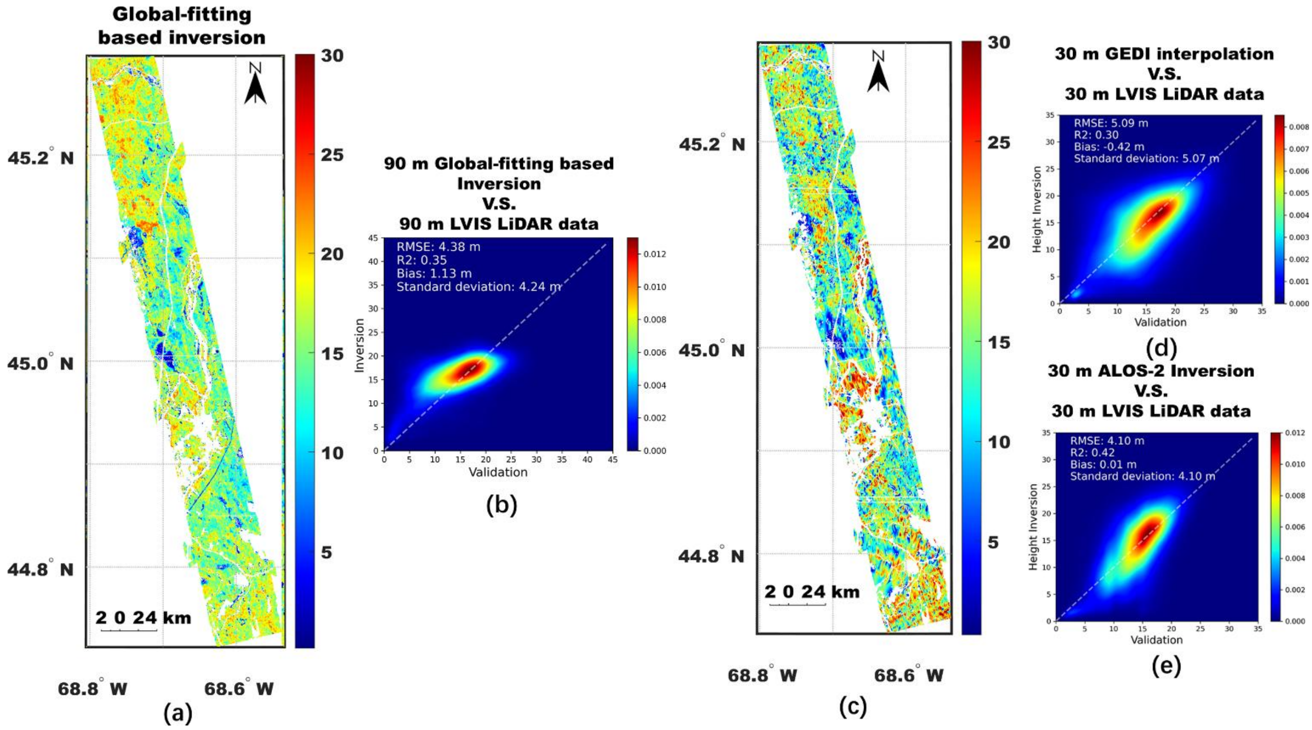


**Figure 20: (a) global-fitting based inversion (Lei et al., 2019) applied to the scene $(S = 0.94, C = 9)$, (b) comparing 90 m gridded maps from (a) with corresponding LVIS data; (c) interpolated 30 m gridded GEDI height map; (d) density scatterplot comparing the interpolated 30 m GEDI map with LVIS LiDAR data; (e) density scatterplot comparing ALOS-2-based inversion results with LVIS LiDAR data.**

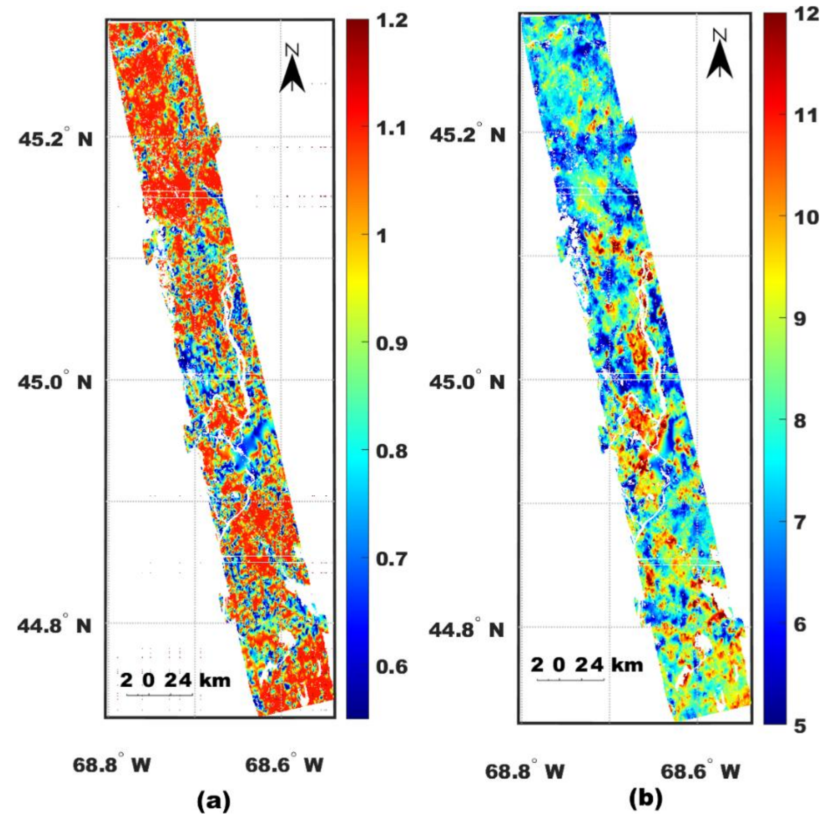


**Figure 21: the interpolated maps of temporal change parameters for (a) *S* and (b) *C***

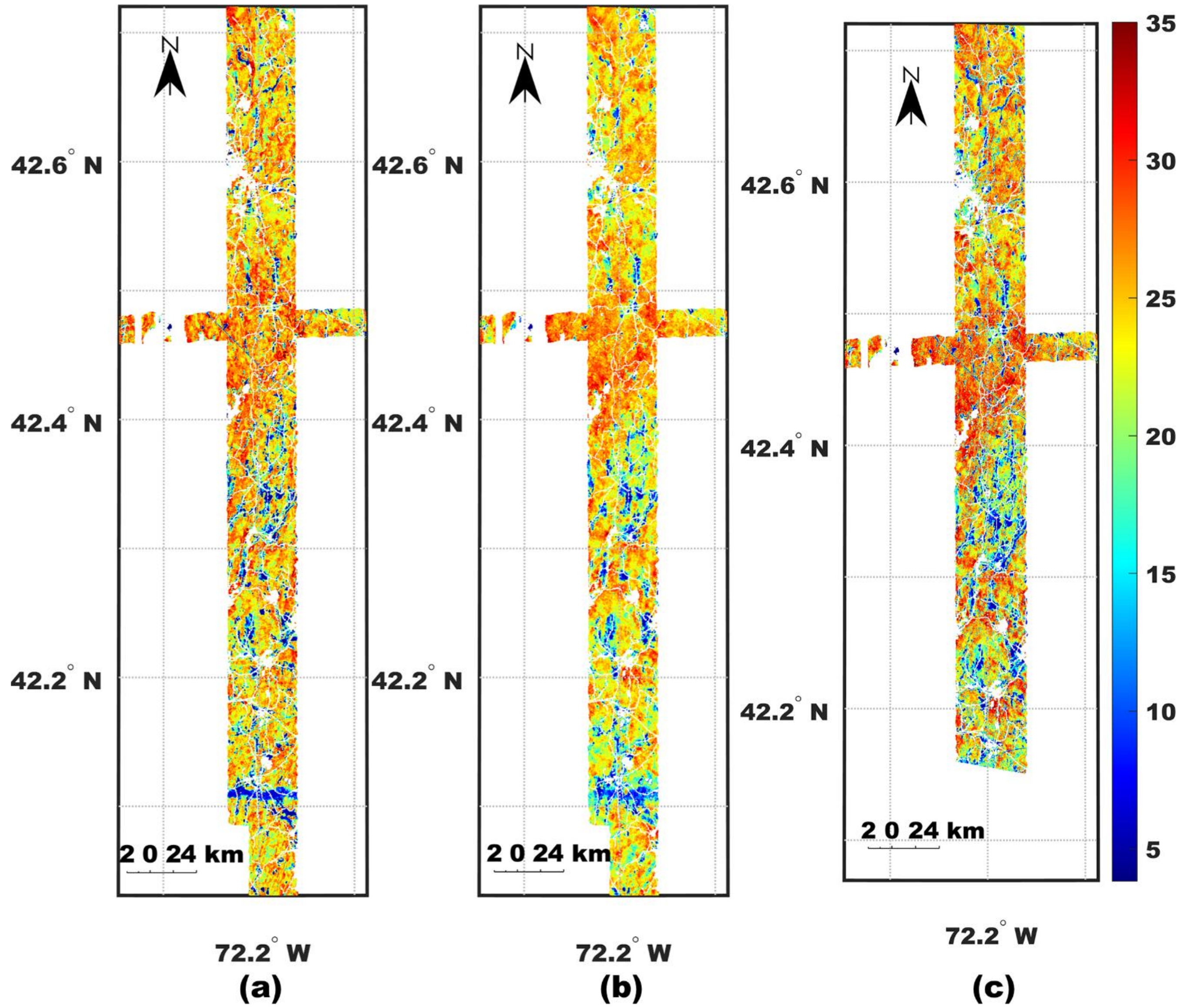


**Figure 22: Validation of 30 m gridded forest height inversion at the Harvard Forest site: (a) LVIS LiDAR RH98, (b) ALOS-1 based estimates (c) ALOS-2 based inversion.**

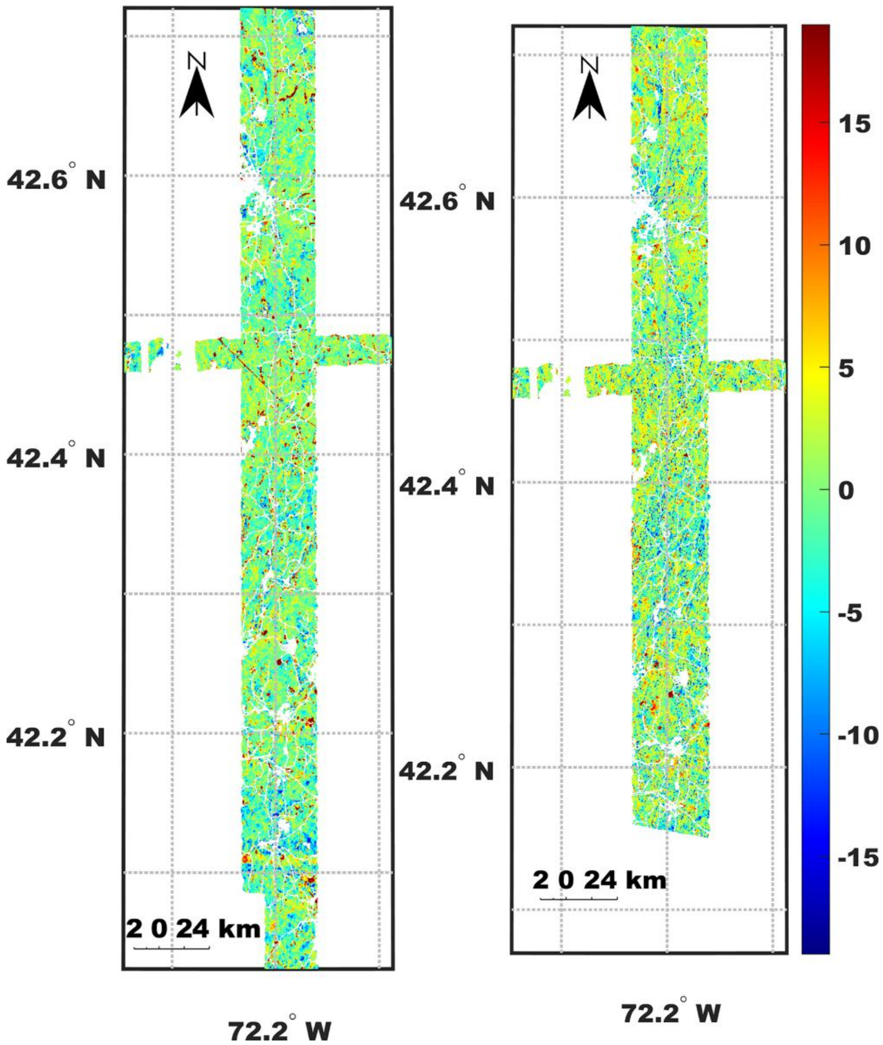


**Figure 23: Differential height maps over the Harvard Forest site: (a) ALOS-1 mosaic versus LVIS LiDAR, and (b) ALOS-2 single scene versus LVIS LiDAR.**

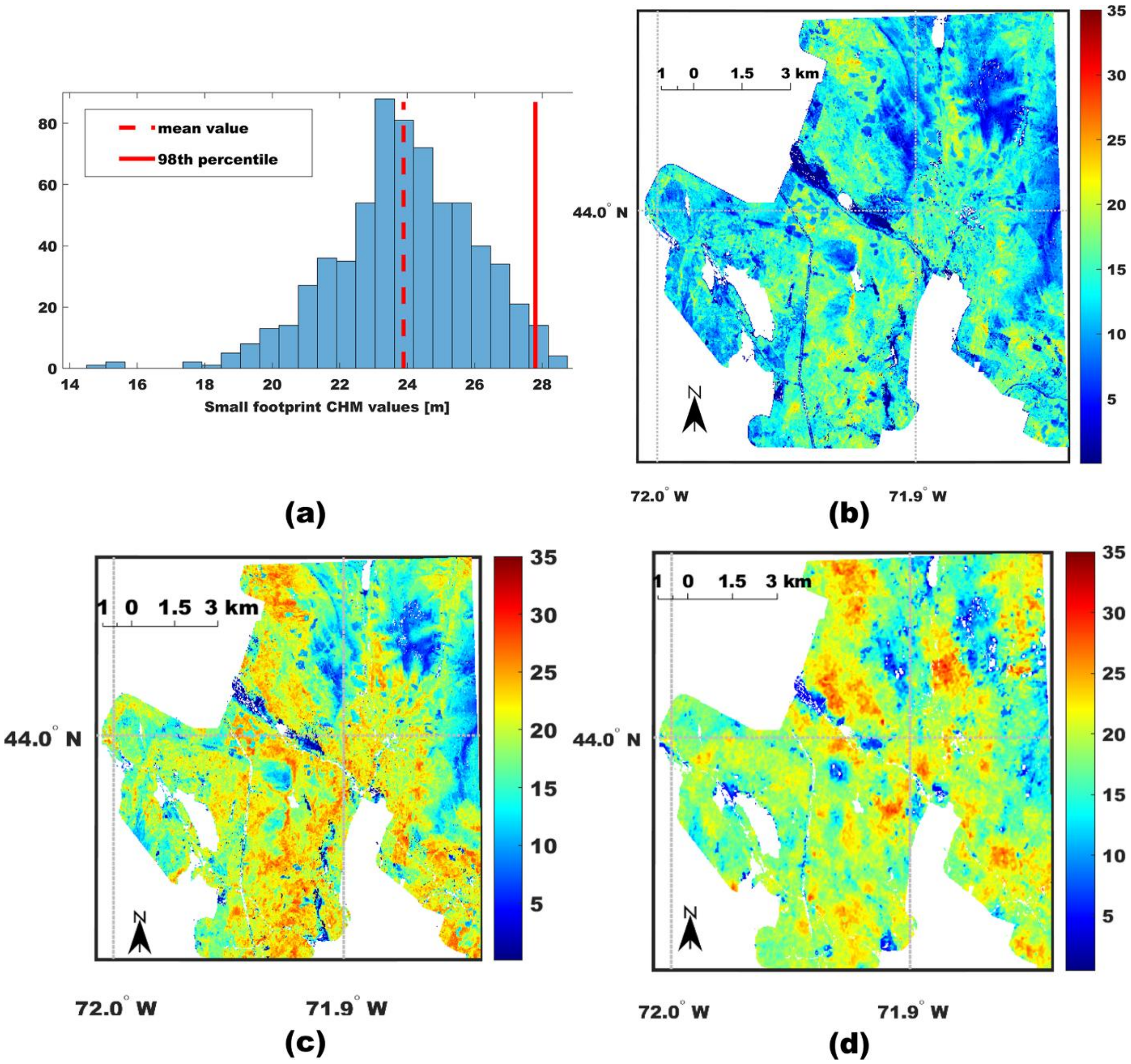


**Figure 24: (a) An example of histogram formed by small footprint CHM values within the GEDI footprint, with mean height and a 98-th percentile height marked by the red dashed and red solid lines, respectively. (b) 30 m gridded reprocessed forest height based on the ERH50 metric, (c) 30 m gridded reprocessed forest height based on the ERH98 metric and (d) corresponding forest height estimates extracted from ALOS-1 mosaic.**

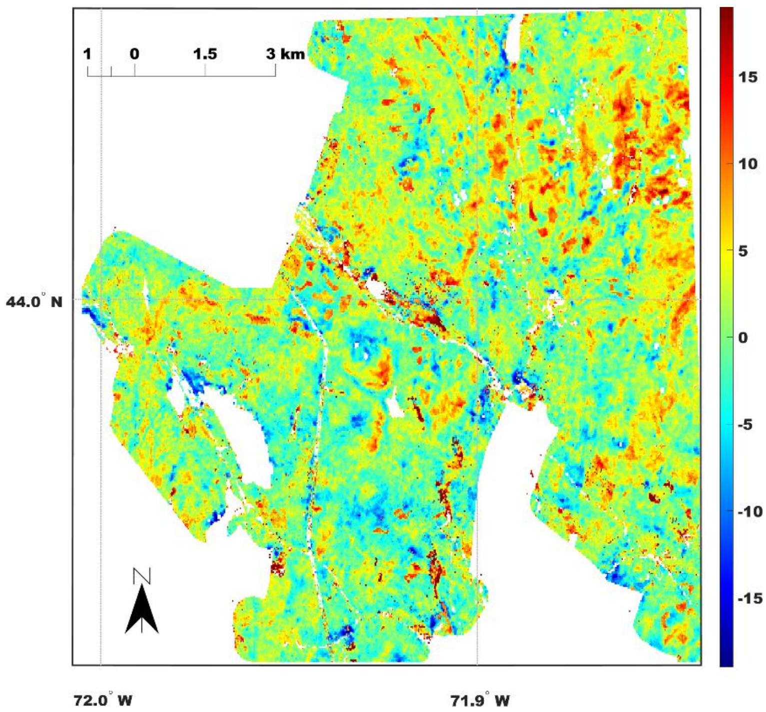


**Figure 25: (a) Differential height map between the ALOS-1 mosaic and GRANIT ERH98 map and (b) the corresponding density scatterplots.**

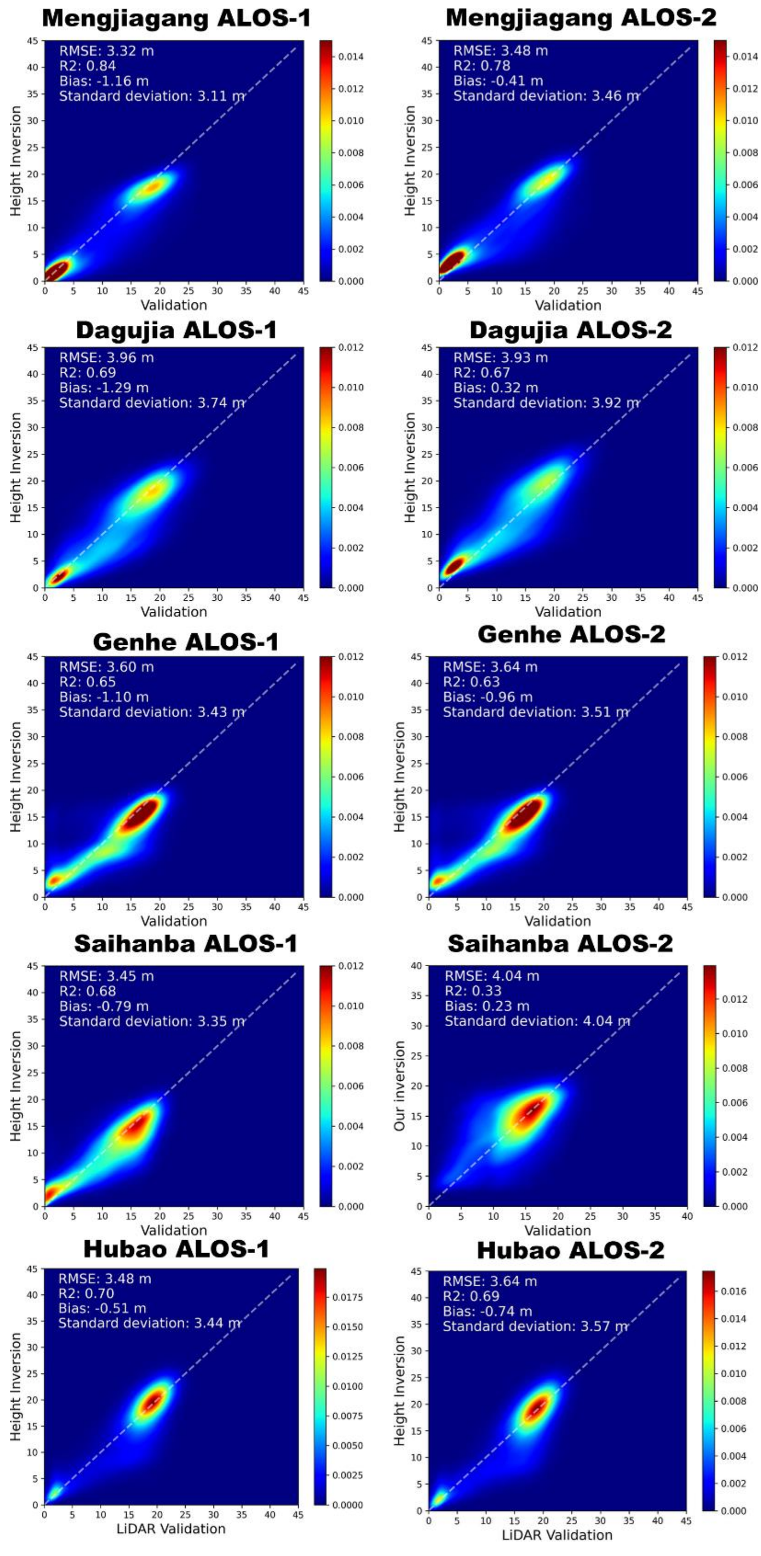


**Figure 26: Density scatterplots comparing LiDAR validation data with forest height inversion estimates across multiple sites of northeastern China based on the ALOS-1 InSAR observation (left panels), and the ALOS-2 observation (right panels).**

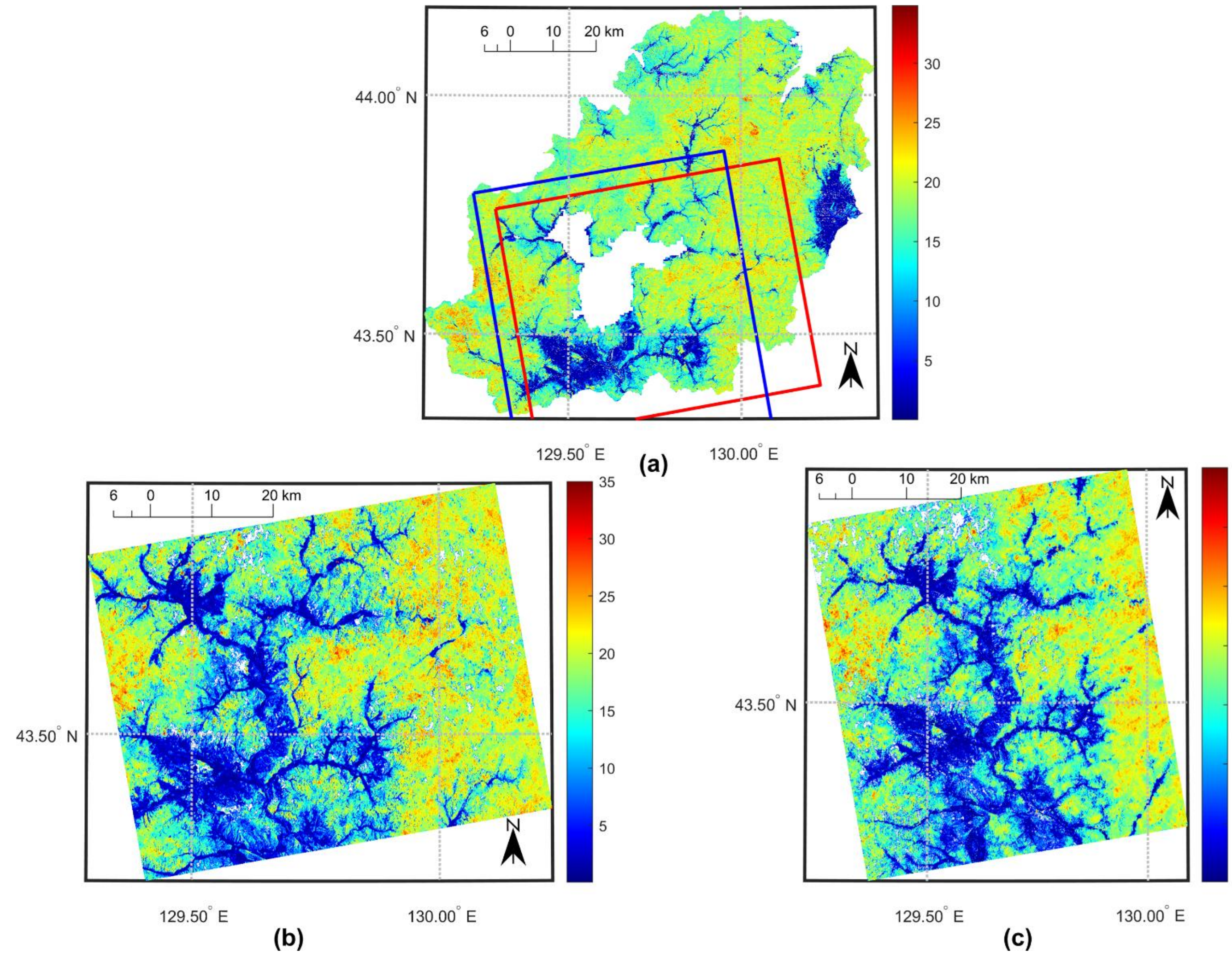


**Figure 27: Comparison of the forest height inversion with LiDAR data at the Hubao National Park site: (a) ALS ERH98 metric map. The red rectangle denotes the coverage of (b) ALOS-1 based single-scene inversion, whereas the blue rectangle indicates the coverage of (c) ALOS-2 based single-scene inversion.**

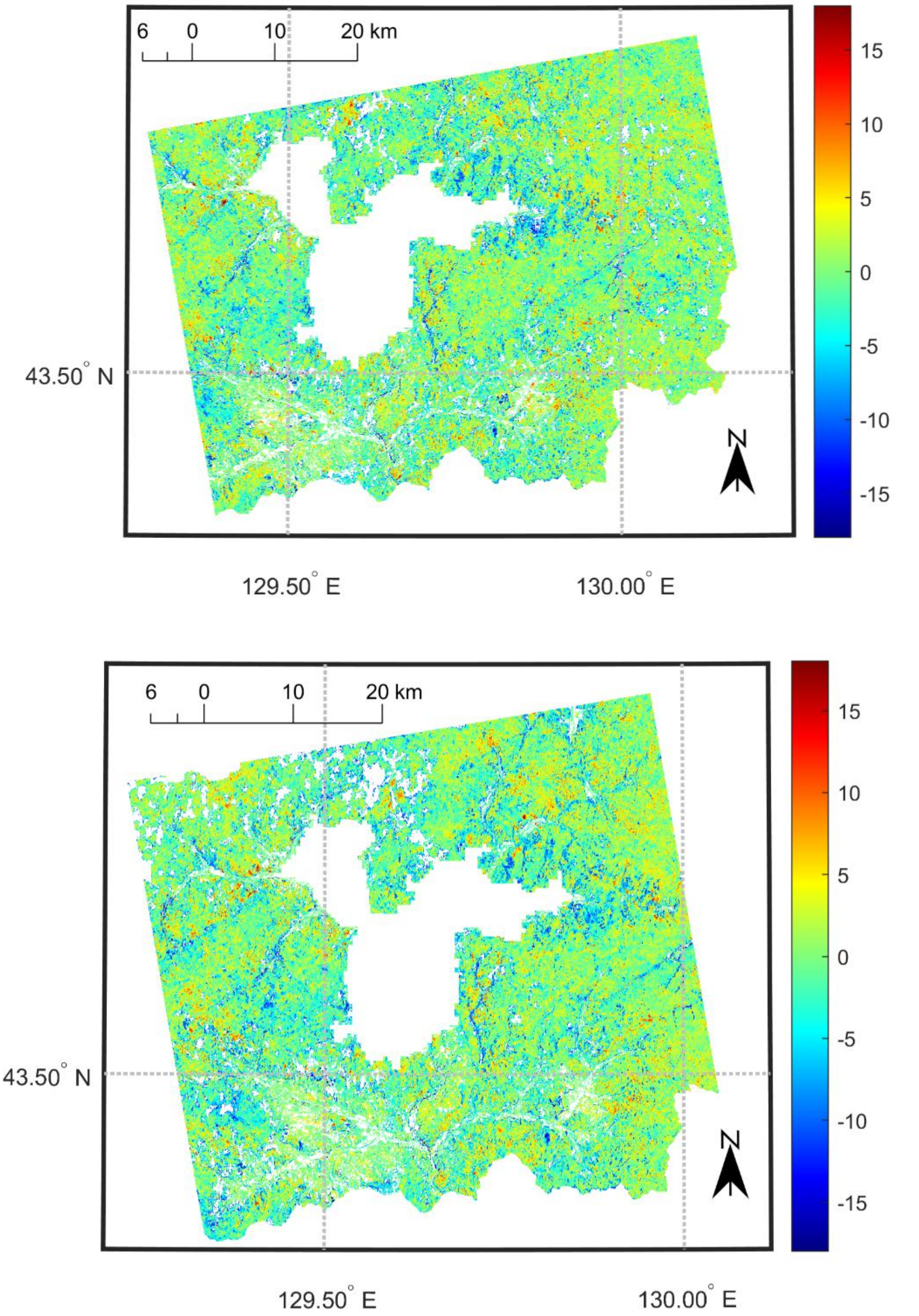


**Figure 28: Differential height map between (Upper panel) the ALOS-1 based inversion and ERH98 validation data, and between (Bottom panel) the ALOS-2 based inversion and ERH98 validation data.**

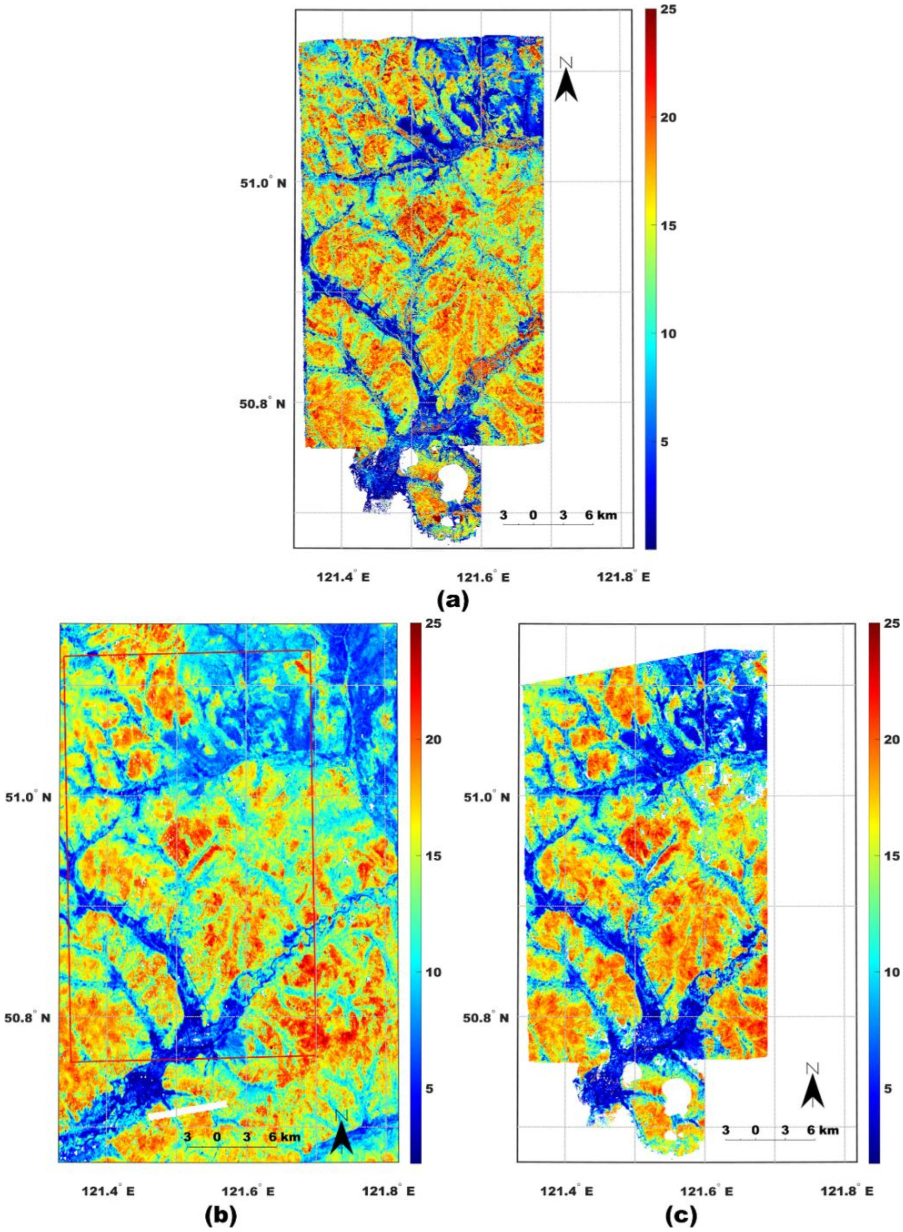


**Figure 29: Comparison of the forest height mapping over the Genhe Forest Bureau: (a) ALS ERH98 metric generated based on 25 m footprint; (b) ALOS-1 mosaic with red rectangle box indicating the overlapping area with (a), and (c) ALOS-2 based single-scene inversion.**

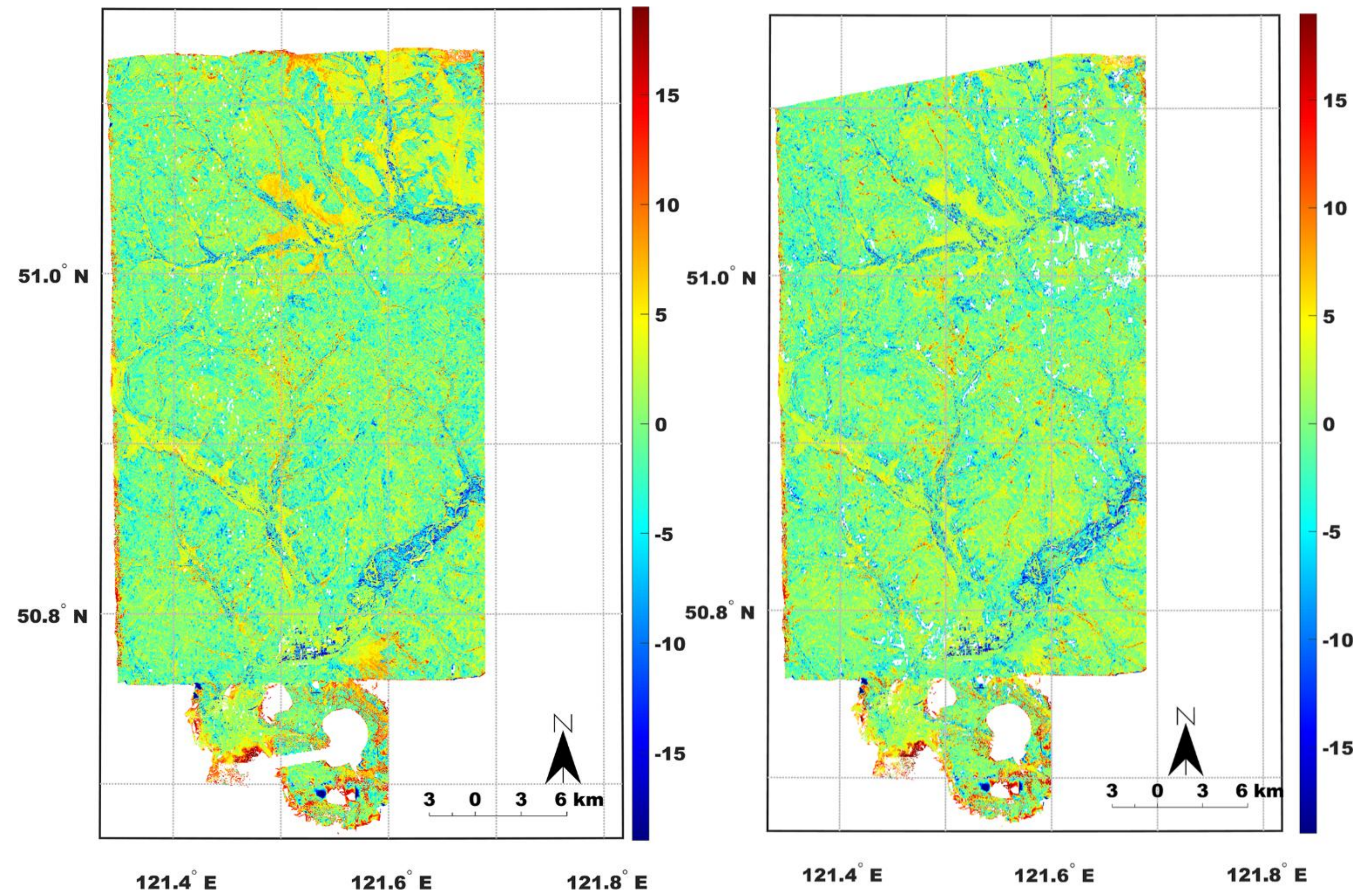


**Figure 30: Differential height map between (left panel) the ALOS-1 based inversion and ERH98 validation data, and between (right panel) the ALOS-2 based inversion and ERH98 validation data.**